RSC Advances

PAPER

View Article Online
View Journal | View Issue

Check for updates

Cite this: *RSC Adv.*, 2021, **11**, 16913

RAFT polymerization mediated core–shell supramolecular assembly of PEGMA-*co*-stearic acid block co-polymer for efficient anticancer drug delivery†

Priyatosh Sarkar,[a] Santanu Ghosh,[ab] Rima Saha[a] and Kishor Sarkar*[a]

In this work, core–shell supramolecular assembly polymeric nano-architectures containing hydrophilic and hydrophobic segments were synthesized *via* reversible addition fragmentation chain transfer (RAFT) polymerization. Herein, polyethylene glycol methyl ether methacrylate (PEGMA), and stearic acid were used to synthesize the poly(PEGMA) homopolymer and stearyl ethyl methacrylate (SEMA), respectively. Then, PEGMA and SEMA were polymerized through controlled RAFT polymerization to obtain the final diblock copolymer, poly(PEGMA-*co*-SEMA) (BCP). Model anticancer drug, doxorubicin (DOX) was loaded on BCPs. Interestingly, efficient DOX release was observed at acidic pH, similar to the cancerous environment pH level. Significant cellular uptake of DOX loaded BCP50 (BCP50-DOX) was observed in MDA-MB-231 triple negative breast cancer cells and resulted in a 35 fold increase in anticancer activity against MDA MB-231 cells compared to free DOX. Scanning electron microscopy (SEM) imaging confirmed the apoptosis mediated cellular death. These core–shell supramolecular assembly polymeric nano-architectures may be an efficient anti-cancer drug delivery system in the future.

Received 2nd March 2021
Accepted 18th April 2021

DOI: 10.1039/d1ra01660a

rsc.li/rsc-advances

Open Access Article. Published on 07 kvtna 2021. Downloaded on 15.04.2026 15:36:47.
This article is licensed under a Creative Commons Attribution-NonCommercial 3.0 Unported Licence.

Introduction

Smart polymeric architectures have opened a new era in the field of biomedical science. Among numerous smart polymeric architectures, the core–shell models have drawn immense research attention, owing to their ability to form self-assembly or micellar structure, for over a decade.[1,2] These smart molecular structures are typically composed of an inner hydrophobic core and an outer hydrophilic shell. Block copolymers have already demonstrated their efficiency to develop such core–shell structures.[3,4] The amalgamation of different monomeric functionalities in one polymer chain leads to successive phase separation along with supramolecular structure formation which can be achieved by various "living" radical polymerization techniques like reversible addition–fragmentation chain transfer (RAFT), nitroxide mediated polymerization (NMP), and atom transfer radical polymerization (ATRP).[5] Among them, RAFT polymerization is the most versatile polymerization technique in terms of monomer versatility as well as a chain transfer agent (CTA) attributed to narrow polydispersity index and controlled molecular weight.[6]

Amphiphilic polymers are generally described as polymers having both hydrophilic and hydrophobic moieties. In an aqueous environment, they can easily form micellar architecture where the outer shell contains hydrophilic moiety and inner core is composed of hydrophobic moiety capable of loading hydrophobic drugs leading to improve the biodistribution and bioavailability of hydrophobic drugs.[7–9] Unlike covalent interactions, the hydrophobic drugs like curcumin, doxorubicin, paclitaxel *etc.* could be easily entrapped inside the hydrophobic core *via* hydrophobic interaction.[9,10]

Nanotechnology has already shown its effectivity in the field of anticancer drug or gene delivery through active or passive targeting.[9,11–16] Unlike active targeting, passive targeting of cancer cells through the faulty vasculature is termed as "enhanced permeation and retention rate" (EPR) where nano-objects are designed to get access to the tumor site through leaky vasculature and accumulate to the tumor, subsequently, nanoparticles enter to the cancer cells *via* endocytosis and release their drug or gene payload.[17,18] Nanoparticles are prone to the process of opsonization by the mono-phagocytic system, whereas, core–shell nanoparticles with an outer hydrophilic shell can easily escape the opsonization process or recognition by "reticuloendothelial system" (RES).[19] Therefore, the incorporation of hydrophilic moiety increases the efficiency of drug delivery to the tumor site by prolonging mean residence time

[a]*Gene Therapy and Tissue Engineering Lab, Department of Polymer Science and Technology, University of Calcutta, 92, A. P. C. Road, Kolkata, 700009, India. E-mail: kishorpst@gmail.com; kspoly@caluniv.ac.in; Web: http://kishorgttl.com; Tel: +91-33-2350-1397 ext. 285*

[b]*Department of Materials Engineering, Indian Institute of Science, C. V. Raman Avenue, Bangalore, Karnataka, 560012, India*

† Electronic supplementary information (ESI) available. See DOI: 10.1039/d1ra01660a

© 2021 The Author(s). Published by the Royal Society of Chemistry

Open Access Article. Published on 07 kvtna 2021. Downloaded on 15.04.2026 15:36:47.
This article is licensed under a Creative Commons Attribution-NonCommercial 3.0 Unported Licence.

(MRT) to the systemic circulation,[20] where, a larger extent of nanoparticle bearing drug molecules can accumulate to the tumor site with weakened lymphatic drainage, whereas permeability to the normal vasculature is restricted due to the tight endothelial junction.[21]

Moreover, the incorporation of fatty acid to a polymeric backbone may lead to an optimal molecular nanostructure for drug delivery application as fatty acids which are saturated or unsaturated long-chain alkyl carboxylic acids, act as a building block of tissue and are also involved in various biological signalling pathways. Stearic acid is one of the long-chain fatty acids having 18 carbon and a terminal carboxylic functional group which could be easily conjugated with various biopolymers for diverse biological applications. Like, Yuan *et al.*[22] prepared stearic acid conjugated chitosan micelle for DOX delivery and evaluated the *in vitro* transport as well as *in vivo* absorption using the Caco-2 cell line. They have found that with the increased stearic acid substitution to the amino group of chitosan greatly influenced the permeability as well as absorption through the gastrointestinal tract. In another study, Hu *et al.*[23] also prepared a shell crosslinked micellar structure by conjugating chitosan with stearic acid and found that the stearic acid hydrophobic core greatly influenced the cellular internalization process. Thus, stearic acid modification of polymer helps to improve the entrapment of the hydrophobic drug by hydrophobic interaction and also influences the release from the inner core.[10] It is believed that physical entrapment of drugs is more favourable than chemical conjugation because a stable covalent bond causes steric hindrance and restrict the enzymatic degradation.[24,25]

The surface engineering of the core–shell model nanoparticle is generally employed to improve the aqueous solubility, stability, to prevent intermolecular aggregation, immunogenicity reduction, and to increase the residence time in the systemic circulation to improve the bioavailability of the hydrophobic drugs.[26] PEG is FDA approved synthetic polymer which is mostly used for hydrophilic modification of the nanoparticles to prevent the RES trapping in the liver and spleen.[20,27–29] For instance, Sun *et al.* prepared a core–shell model nanoparticle to understand the effect of PEGylation and observed that biodistribution of PEGylated nanoparticles was higher with long circulation time into the systemic circulation.[30]

An optimal nano-drug delivery system includes well dispersibility, high drug payload, adequate biocompatibility, which could be achieved by the amalgamation of lipid and hydrophilic polymer to overcome the shortcomings associated with only lipid or polymer-based nanoparticles. Therefore in this study, we adopted RAFT polymerization to prepare poly(-poly(ethylene glycol) methyl ether methacrylate-*co*-stearyl ethyl methacrylate) (poly(PEGMA-*co*-SEMA)) block copolymer having controlled molecular weight, which could able to form core–shell structure in the aqueous environment. Anticancer drug DOX was loaded to the hydrophobic SEMA core by physical entrapment. The effect of increased hydrophobic SEMA part in the block copolymer system on DOX loading was evaluated along with the evaluation of their corresponding biocompatibility, cellular uptake study and *in vitro* anticancer activity against MDA-MB 231 as a model cancer cell line.

Materials & methods

Sodium hydride, 1-dodecanethiol, 4,4-azobis(4-cyanovaleric acid), deuterated chloroform ($CDCl_3$), 2-hydroxy ethyl methacrylate (HEMA), polyethylene glycol methyl ether methacrylate −300 (PEGMA), pyrene, and MTT were purchased from Sigma Aldrich (Germany) and were used without further purification. Stearic acid, DMEM media, and molecular biology grade water, fetal bovine serum (Brazil origin, EU approved), and trypsin-EDTA were purchased from Himedia laboratories private limited (Mumbai, India). Doxorubicin HCl was purchased from Tokyo Chemical Industry, (Japan). Dicyclohexylcarbodimide (DCC), 4-dimethylaminopyridine (DMAP) were purchased from SRL chemicals (Mumbai, India). 2,20-Azo-bis-(isobutyronitrile) (AIBN) were purchased from SRL and were recrystallized from methanol before use. Fluorescent probes pyrene and DAPI were purchased from Sigma Aldrich (Germany). All the solvents were used as purchased without any further purification.

Synthesis of chain transfer agent (CTA)

The CTA, 4-cyano-4-(dodecylsulphanylthiocarbonyl) sulphanyl pentanoic acid (CDSP) and was prepared according to Saha *et al.*[31] In brief, sodium hydride (NaH, 0.62 g, 25.8 mmol) was dissolved in diethyl ether (50 ml) into a three-neck jacketed reactor under nitrogen condition at 5–10 °C, 1-dodecanethiol (5 g, 24.7 mmol) was added slowly to that solution to obtain sodium dodecylate as thick white slurry and the temperature was cooled down to 0 °C. After that carbon disulphide (CS_2, 1.9 g, 24.9 mmol) was added dropwise to the reaction mixture which leads to the formation of sodium *S*-dodecyl trithiocarbonate. The resulted yellowish product was filtered and dried under a vacuum oven at room temperature for further reaction. In the next step, solid iodine granules (2.54 g, 10 mmol) were added to diethyl ether solution (40 ml) of sodium *S*-dodecyl trithiocarbonate (5.96 g, 19.8 mmol) in a portion-wise manner under continuous stirring and allowed to stirr for a further 1 hour at room temperature. Sodium iodide as a by-product was filtered off; subsequently, the yellowish solution was collected and washed by sodium thiosulfate followed by anhydrous sodium sulphate. The collected filtrate solution was concentrated using a rotary evaporator (Heidolph, Germany) to obtain bis(dodecylsulfanylthiocarbonyl) disulphide. Then the dried bis(dodecylsulfanylthiocarbonyl) disulphide (3 g, 5.4 mmol) was refluxed using ethyl acetate (55 ml) in presence of 4,4-azobis(4-cyanovaleric acid) in ethyl acetate for 18 hours. Subsequently, the crude CDSP was extracted with water and recrystallized from cold hexane (yield = 83%). The structural characterization of purified CDSP was confirmed by ^{1}H NMR.

Synthesis of stearyl ethyl methacrylate (SEMA)

SEMA was synthesized according to Maiti *et al.*[32] Briefly, in a two-neck round bottom flask, stearic acid (SA) was dissolved into dry dichloromethane (DCM). Nitrogen was purged into the reaction mixture while the flask was kept in an ice bath. DCC was separately dissolved into dry DCM and added to the reaction mixture. After 30 min DMAP was added followed by

© 2021 The Author(s). Published by the Royal Society of Chemistry

Open Access Article. Published on 07 kvtna 2021. Downloaded on 15.04.2026 15:36:47.
This article is licensed under a Creative Commons Attribution-NonCommercial 3.0 Unported Licence.

dropwise addition of HEMA for 15 min. The ice bath was removed after 30 min and the reaction was allowed to stir under a nitrogen environment for 24 hours. After 24 hours, the formed dicyclohexyl urea (DCU) was removed by filtration. The obtained clear organic solution was separated by several times washing with saturated $NaHCO_3$ solution (3 × 100 ml) followed by washing with brine solution (3 × 100 ml). The washed organic solution was dried over sodium sulphate and DCM was removed under reduced pressure by a rotary evaporator. Finally, the product was purified using silica gel (230–400 mesh size) flash column chromatography using ethyl acetate : hexane.

RAFT polymerization

Synthesis of homopolymer. Poly (ethylene glycol) methyl ether methacrylate (PEGMA) was synthesized *via* RAFT polymerization. Here, we have used CDSP as a RAFT reagent which is a well known for various polymer synthesis *via* RAFT polymerization.[31] CDSP was dissolved in dry DMF with continuous nitrogen purging. After that, PEGMA and AIBN were added to the reaction mixture. After 30 min, the reaction mixture was placed in an oil bath and the reaction was carried out at 70 °C for another 12 hours in nitrogen environment. After polymerization takes place the reaction mixture which contains both poly(PEGMA) and unreacted PEGMA was dissolved in DCM and precipitated into hexane to remove unreacted PEGMA. The poly(PEGMA) was further used for the block copolymer synthesis.

Synthesis of block co-polymer. After the successful synthesis of the homopolymer, the block co-polymer was synthesized using the synthesized SEMA monomer. Briefly, poly(PEGMA) was dissolved in dry DMF with continuous nitrogen purging. Then the required amount of SEMA and AIBN was dissolved in dry DMF and injected into the reaction mixture and allowed to stir under continuous nitrogen purging for 30 min. After that, the reaction mixture was placed in a preheated oil bath at 60 °C with continuous stirring for 7 hours. To stop the reaction the solution was cooled down to 4 °C and the crude polymeric solution was dialyzed against methanol to remove unreacted monomer by changing methanol after every 3 hours for 36 hours. Finally, the synthesized polymer was dried overnight in a vacuum oven at 40 °C. We have prepared all the block copolymer according to the SEMA feed ratio with homopolymer poly(PEGMA) as (SEMA : poly(PEGMA)) 10 : 1 (BCP10), 25 : 1 (BCP25) and 50 : 1 (BCP50).

Characterization. UV-Vis spectra of BCP and DOX loaded BCP at 100 μg ml^{-1} concentration in water have been recorded with Perkin Elmer Lambda 65 spectrophotometer within the range of 200–800 nm (typically quartz cuvette, 1 cm path length) at 25 °C temperature. The synthesized BCP was also characterized by NMR (Bruker, 500 MHz, Germany) and FT-IR spectroscopy (Perkin Elmer Spectrum-2). All FT-IR spectra were carried out within the frequency range of 4000 to 600 cm^{-1} with a scan rate of 8 consecutive scans at 1 cm^{-1} resolution. Transmission electron microscopy (TEM) was carried out after depositing of BCP aqueous solution on a carbon-coated Cu grid and subsequently the images were taken by JEM-2100F (JEOL, Japan) operating at 200 kV. Micelle size and zeta potential of BCP and DOX loaded BCP was measured using Zetasizer Nano ZS, Malvern Panalytical Ltd, UK at 25 °C using a disposable 12 mm square polystyrene cuvette and disposable folded capillary cell at 1 mg ml^{-1} concentration. Confocal laser scanning microscopy (CLSM) images were taken using an FV3000, Olympus at 405 and 559 nm excitation wavelength at 25 °C. Scanning electron microscopy (SEM) images were also taken using ZEISS, EVO-18 special edition, Germany.

Preparation of doxorubicin (DOX) loaded BCP micelles

DOX was loaded into the core of the nanoparticle by physical entrapment *via* film hydration method according to Wei *et al.*[33] with minor modification. Briefly, hydrophobic DOX was obtained by neutralizing DOX. HCl using trimethylamine (1 : 3 mole ratio) in 1 ml of a mixed solvent of chloroform : methanol (3 : 2). Then the resulting solution was mixed with the different mass ratios of BCPs (BCP : DOX = 1 : 0.1, 1 : 0.5, 1 : 1) followed by evaporation using a rotary vacuum evaporator to obtain a thin film on the surface of the round bottom flask. Then, the dried film was hydrated using a 10 mM HEPES buffer and stirred at 60 °C for 30 min. The DOX encapsulated BCPs were then dialyzed (dialysis tube molecular cutoff 3.5 kDa) against DD water for 9 hours in dark conditions to remove the unentrapped DOX with a continuous exchange of fresh DD water after every hour. The obtained product was then lyophilized and stored at 4 °C for further investigation. The encapsulated DOX content was quantified by UV-Vis spectroscopy and DOX encapsulated BCPs were screened according to the highest drug loading (%) and encapsulation efficiency which was calculated from the following formula.

$$\text{Drug loading } (\%) = \frac{M_t}{M_s} \times 100\%$$

$$\text{Encapsulation efficiency } (\%) = \frac{M_t}{M_0} \times 100\%$$

M_t = mass of DOX encapsulated into the BCP, M_s = mass of the DOX loaded BCP after lyophilization, M_0 = initial mass of DOX feed.

In vitro DOX release study

An *in vitro* drug release study was conducted to evaluate the release pattern of DOX from the core of the nanoparticles at different pH (5 and 7.4) environments. DOX release pattern was observed using a dialysis membrane tube (10 kDa) at 37 °C in a dynamic environment.[34] Briefly, DOX loaded BCP50 (contains 280 μg of DOX) was dispersed into freshly prepared phosphate buffer saline (PBS) of different pH and placed into a dialysis tube. Then, the dialysis tube was immersed into 15 ml PBS with continuous stirring at low rpm. To maintain sink condition, 2 ml of PBS buffer was withdrawn from the external chamber after a predetermined time interval (0, 0.5, 1, 2, 4, 6, 8, 10, 12, 24, 48, 72, 96, 120 h) and replaced with fresh PBS. The absorbance was measured at 481 nm using a UV-Vis

Open Access Article. Published on 07 kvtna 2021. Downloaded on 15.04.2026 15:36:47.
This article is licensed under a Creative Commons Attribution-NonCommercial 3.0 Unported Licence.

spectrophotometer. From the obtained absorbance% cumulative DOX release was calculated. All the experiments were performed in triplicate with ±SD. Different release kinetics models such as zero order, first order, Hixon–Crowell, Korsmeyer–Peppas and Higuchi model was also employed to evaluate the DOX release mechanism from the nanoparticle.[35]

Cell culture. Doxorubicin sensitive MDA-MB 231 (human epithelial triple-negative breast cancer cell line) was purchased from the National center for cell science (NCCS), Pune, India. *In vitro* cell cytotoxicity assay was done by using MTT to understand the growth of cancer cells upon free polymer as a placebo at different concentrations, intracellular uptake of DOX loaded nanoparticle and cellular morphology with DOX loaded nanoparticle after 24 hours using SEM was conducted according to standard established protocol. Cells were grown in DMEM media and maintained at 5% CO_2 and 37 °C using a CO_2 incubator (CelCulture, ESCO, Singapore) according to the supplier protocol. DMEM media with 10% FBS, 1% penicillin–streptomycin, 2 mM L-glutamine was used as a supplement.

Cell viability assay. To evaluate the cytotoxicity of BCPs and DOX loaded BCPs, MTT assay was performed against MDA-MB 231 cell lines. Briefly, cells were seeded to 96 well plates at a density of 10^3 cells per 100 μl DMEM media followed by 24 hours incubation in a 5% CO_2 incubator. The samples contain BCPs with or without DOX were prepared using fresh media with a sample concentration varied from 10, 25, 50, 100, 200, and 500 μg ml^{-1}. After the incubation period, the cells were introduced to the polymer solution prepared using fresh media and further incubated for another 24 hours. MTT solution at a concentration of 50 μg ml^{-1} was added to each well followed by 4 hours of incubation. After completion of 4 hours of incubation media containing MTT solution was carefully replaced with 100 μl of DMSO into each well and allowed to shake for 15 in the dark and absorbance was recorded using an ELISA plate reader at 570 nm wavelength. The % cell viability was calculated according to the following formula. All the cytotoxicity study was performed in triplicate with ±SD.

$$\text{Cell viability } (\%) = \frac{OD_{570(Sample)}}{OD_{570(Control)}} \times 100$$

where $OD_{570(Sample)}$ and $OD_{570(Control)}$ refers to the absorbance of sample and control at 570 nm.

Cellular uptake study. To perform the uptake study of nanoconjugates MDA-MB-231 cells were used in a 24 well plate. 1×10^5 cells were seeded on a sterile glass coverslip which was placed in each well of a 24 well plate and incubated in a CO_2 incubator (37 °C, 5% CO_2, 95% RH) for 24 hours. Replenishment of media the DOX and DOX loaded BCP at a concentration of 100 μg ml^{-1} conjugates were added to each well followed by 4 h incubation at CO_2 incubator. Thereafter, completion of the 4 hours incubation period the media was removed and the cells were washed with DPBS to ensure removal of free nanoconjugates which were not uptaken by the cells. 4% paraformaldehyde was used to fix the cells and followed by DPBS was for 3 times. The washed coverslips were carefully removed from the well plate and inversely mounted on a clean glass slide upon drop of glycerol which acts as a mounting media.

Determination of cellular morphology by scanning electron microscopic (SEM) images. Cellular morphology after treatment using DOX loaded BCP and DOX was observed under the scanning electron microscope (SEM) to understand the morphological changes with respect to untreated cells as control. The study was conducted according to Basu *et al.*[36] with some modification. Briefly, the glass coverslips washed with 70% ethanol followed by PBS wash (3 times) were placed in each well of a 24 well plate. 2×10^3 no of cells in 400 μl of DMEM media were seeded on a previously placed glass coverslip in each well and placed in a CO_2 incubator for 24 h. After 24 h the media was replenished with fresh media containing BCP/DOX and DOX followed by a further 24 h incubation period in a CO_2 incubator. After 24 h of incubation, the cells were washed with PBS (300 μl × 3 times) to remove the non-internalized BCP/DOX and DOX. The cells were subjected to fixation using 4% paraformaldehyde to stop the metabolic activity of the corresponding cells. Prior to SEM analysis, cells were dehydrated using a sequential gradation of ethanol (10%, 30%, 50%, 70%, 90%, and absolute ethanol) followed by air-dry at room temperature. The coverslips were observed under SEM.

Result and discussion

Synthesis and characterizations of the monomer and polymers

Characterization of CTA. The successful synthesis of CDSP was confirmed by ^{1}H NMR analysis (Fig. S2†). The observed characteristic ^{1}H NMR spectra of CDSP were as follows:

^{1}H NMR, 500 mHz, $CDCl_3$, δ(ppm): COOH–CH_2–CH_2–C(CN)(CH_3)–S–(C=S)–S–$C_{11}H_{23}$–CH_3-0.882(3H); COOH–CH_2–CH_2–C(CN)(CH_3)–S–(C=S)–S–CH_2–$CH_2C_9H_{18}$–CH_3-1.24(18H), COOH–CH_2–CH_2–C(CN)(CH_3)–S–(C=S)–S–CH_2–$CH_2C_9H_{18}$–CH_3-1.7(2H); COOH–CH_2–CH_2–C(CN)(CH_3)–S(C=S)–S–CH_2–$CH_2C_9H_{18}$–CH_3-1.87(3H); COOH–CH_2–CH_2–C(CN)(CH_3)–S–(C=S)–S–CH_2–$CH_2C_9H_{18}$–CH_3-2.64–2.7(4H); COOH–CH_2–CH_2–C(CN)(CH_3)–S–(C=S)–S–CH_2–$CH_2C_9H_{18}$–CH_3-3.31(2H). The ^{1}H NMR spectra of CDSP shows similar chemical shifts which is reported earlier in our previous research.[31]

Monomer synthesis. SEMA was synthesized *via* esterification reaction between (SA) and 2-HEMA (Fig. S1†). In this reaction –COOH terminal of SA was reacted with –OH functional group of 2-HEMA with 60% yield. The structure of the synthesized monomer was confirmed by ^{1}H NMR spectroscopy. All the peaks have been assigned to their corresponding proton shown in Fig. S3† which were in accordance to previous report.[32] The resonance for vinyl protons present in the SEMA structure (C=CH_2, 2H) have been observed at δ (ppm) 6.15 and 5.60. End methyl group of the long aliphatic chain came at 0.9 ppm which is quite expected (marked as 'h'), sharp peaks in between 1.3–1.7 ppm (marked as f and g) corresponds to methylene protons of the SEMA unit. –CH_2 proton adjacent to –(CO) group of SEMA unit came at relatively downfield region of 2.4 ppm (marked as e) due to attachment of electron withdrawing –O(CO)R group. A sharp peak at 4.4 ppm (marked as c and d) corresponds to CH_2–CH_2 protons which is flanked between two oxygen atoms of HEMA unit.

© 2021 The Author(s). Published by the Royal Society of Chemistry

Open Access Article. Published on 07 kvtna 2021. Downloaded on 15.04.2026 15:36:47.
This article is licensed under a Creative Commons Attribution-NonCommercial 3.0 Unported Licence.

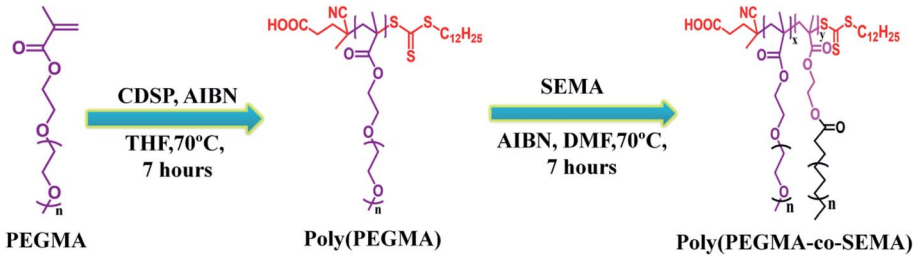

Fig. 1 Synthesis route of PEGMA-*co*-SEMA block co-polymer.

Poly(PEGMA) synthesis. As shown in Fig. 1, the synthetic route depicts the synthesized block copolymer consisting of PEGMA and long-chain fatty acid repeating unit. RAFT polymerization was employed to obtain polymers with controlled molecular weight as well as a defined chain terminal,[37] herein we also have used RAFT polymerization technique to obtain core–shell lipid polymer hybrid nanoparticle for drug delivery application using CDSP as CTA. The homopolymer poly(-PEGMA) was synthesized by using CTA and AIBN as a thermal initiator at a feed ratio of PEGMA : CDSP : AIBN = 50 : 1 : 0.25. ^{1}H NMR spectra for poly(PEGMA) (Fig. 2a) shows the complete disappearance of vinyl proton in the corresponding region and all the peaks have been assigned to their respective structure. The poly(PEGMA) shows resonance signal at 4.02 ppm for O–CH_2–CH_2–O, 3.64 ppm for CH_2–O–(CH_2–CH_2)$_n$, 3.38 ppm for O–CH_3 which are characteristic peak for poly(PEGMA).[32,38,39] The molecular weight based on end group analysis was calculated by comparing the integral area acquired by the CTA at 2.29–2.48 ppm which corresponds to the COOH–CH_2–CH_2–C(CN)(CH_3)– and the area acquired by the repeating unit of poly(PEGMA) at 3.38 ppm. The degree of polymerization (D_p^n) value for poly(PEGMA) was found 26.9–27 and the calculated molecular weight was 7877 g mol^{-1} (ref. [38]) (Table 1). The theoretical molecular weight ($M_{n,theo}$) of the homopolymer was also calculated according to the following formula and was found 9763 g mol^{-1} which is in good agreement with the molecular weight obtained by $M_{n,NMR}$.

$$M_{n,theo}=(([SEMA]/[CDSP] \times M_W \text{ of SEMA} \times \text{conversion}) + (\text{molecular weight of CDSP}))$$

Synthesis of poly(PEGMA-*co*-SEMA). Block copolymers were synthesized with different mole ratio to poly(PEGMA) as a macro CTA (mCTA) which are SEMA : mCTA : AIBN = 10 : 0.1 : 0.025, 25 : 0.1 : 0.025 and 50 : 0.1 : 0.025. Copolymers were obtained by dialysis against methanol to remove unreacted monomer using a 3.5 kDa dialysis membrane to get purified BCP and the ^{1}H NMR spectra also show the complete disappearance of the vinyl proton to the corresponding NMR spectra Fig. 2c. The typical ^{1}H NMR spectrum of poly(PEGMA-*co*-SEMA) block copolymer (Fig. 2b) shows the proton signal at 4.20–4.31 ppm for –O–CH_2–CH_2–O– of SEMA monomer, 2.33 ppm for

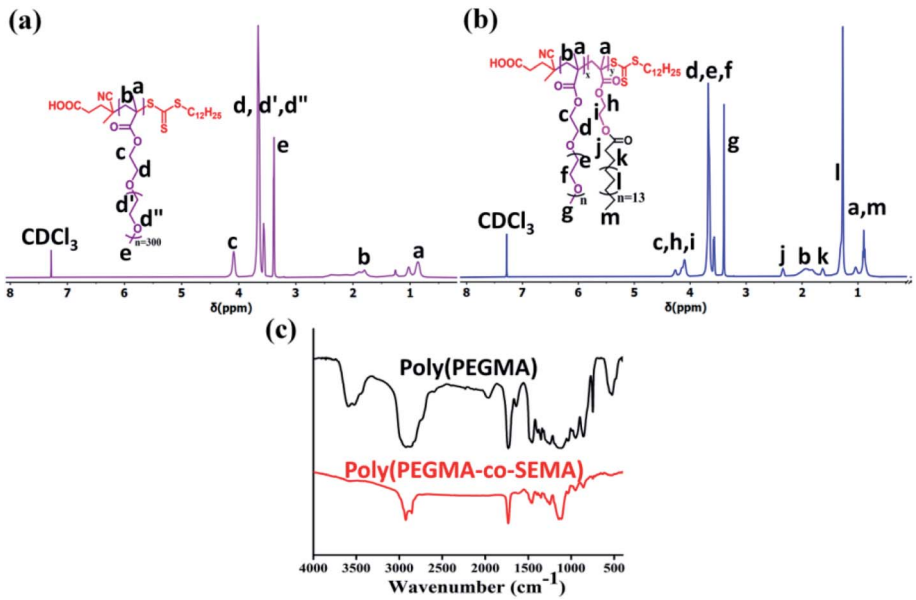

Fig. 2 ^{1}H NMR spectra of synthesized (a) poly(PEGMA) (b) poly(PEGMA-*co*-SEMA) (BCP50) polymer and (c) FTIR spectra of poly(PEGMA) and poly(PEGMA-*co*-SEMA) (BCP50) polymer.

Open Access Article. Published on 07 kvtna 2021. Downloaded on 15.04.2026 15:36:47.
This article is licensed under a Creative Commons Attribution-NonCommercial 3.0 Unported Licence.

Table 1 Molecular weight distribution of the synthesized polymer

Polymer	SAMA content	Time (h)	Conv.[a] (%)	$M_{n,theo}$[b] (g mol^{-1})	$M_{n,NMR}$[c] (g mol^{-1})	D_P[nd]
Poly(PEGMA)	0	12	78	9763	7877	27
BCP10	10	7	53	8400	10 523	7
BCP25	25	7	50.7	12 903	14 187	15
BCP50	50	7	59	20 369	15 809	20

[a] Calculated by ^{1}H NMR spectroscopy. [b] Theoretical molecular weight ($M_{n,theo}$) = ([M]$_0$/[CTA]$_0$ × molecular weight (M_W) of [M]) × conversion+ (M_W of CTA). [c] Molecular weight calculated from ^{1}H NMR spectroscopy. [d] Obtained by ^{1}H NMR spectroscopy.

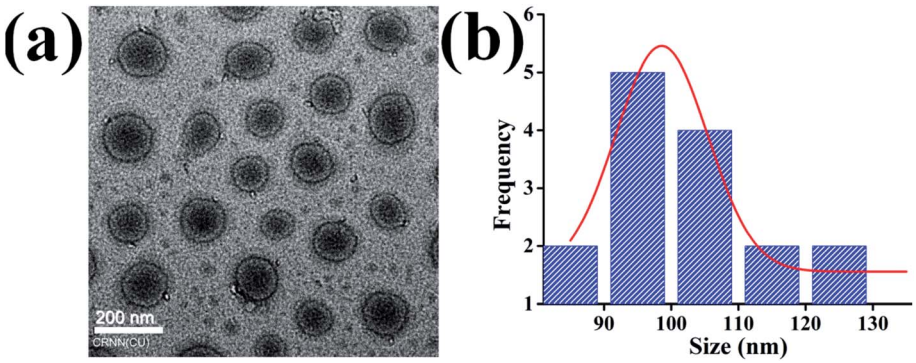

Fig. 3 (a) Transmission electron microscopy (TEM) image of core–shell BCP nanoparticles (b) size distribution of BCP50.

O–C=O–CH_2–CH_2–$(CH_2)_{13}$–CH_2–CH_3, 1.62 ppm for O–C=O–CH_2–CH_2–$(CH_2)_{13}$–CH_2–CH_3, 1.26 ppm for O–C=O–CH_2–CH_2–$(CH_2)_{13}$–CH_2–CH_3 and 0.87 ppm for O–C=O–CH_2–CH_2–$(CH_2)_{13}$–CH_2–CH_3.

The calculated molecular weight of different BCPs is also gradually increasing along with the increase of SEMA monomer feed ratio as the (Table 1). To calculate the molecular weight here we have compared the integral area acquired by the end group of CTA (COOH–CH_2–CH_2–C(CN)(CH_3)–) at 2.29–2.48 ppm and the integral area acquired by the SEMA (–O–CH_2–CH_2–O–) repeating unit at 4.20–4.31 ppm.[38,40] Theoretical molecular weight ($M_{n,theo}$) shows a close resemblance with the molecular weight calculated from NMR ($M_{n,NMR}$) (Table 1).

Size and morphology of the micelle

Di-block BCPs containing both hydrophobic and hydrophilic blocks are expected to form a stable nanostructure in the aqueous solution where hydrophobes will remain inward to form the core and hydrophilic segment will form a corona. The polymeric chain will self-assemble or will aggregate at a certain concentration commonly termed as critical micelle concentration (CMC) or critical aggregation concentration (CAC). To assess the self-assembled core–shell structure of the synthesized BCPs namely BCP10, BCP25, and BCP50 (1 mg ml^{-1}) in an aqueous environment were studied using hydrodynamic size measurement by DLS and the core–shell morphology of the nanoparticle was investigated by TEM. Fig. 3a shows the regular shape nanoparticle morphology of BCP50 and the size distribution curve shows maximum nanoparticles are within size range from 90–100 nm (Fig. 3b). Fig. 3a shows the structural morphology of BCP where a dark dense inner core and an outer ring-like shell structure is present due to hydrophobic segment SEMA and hydrophilic PEGMA repeating units respectively. The morphology could be defined as a core–shell nanostructure and are beneficial for hydrophobic drug delivery application as the shell act as a shield to the inner core from easy degradation by acidic environment present at the tumor site[33] which may lead to prolong release of DOX.

The DLS measurement of the nanoparticle shows a significant increment in their size with the increase of SEMA repeating unit whereas dox loaded nanoparticles also show increased diameter accordingly (Table 2). The increase in hydrophobes requires more space to accommodate the long-chain fatty acids. DLS measurement shows nanoparticles are slightly increased in size than TEM images, which is due to the encrusted water to the surface of the PEGMA corona, in case of TEM image the nanoparticles are dehydrated. It is also noted that the hydrodynamic size difference between blank BCPs and DOX loaded BCPs is due to the expansion of the inner core with high drug payload and strong hydrophobic interaction between DOX and stearic acid long chain. It is acknowledged that the miscibility between the hydrophobic segment and hydrophobic drug also increases the cargo load whereas lipid polymeric hybrid micelle containing higher hydrophobic long-chain should solubilize more DOX with increased micellar structure.[39,41] The observed zeta potential for with or without drugs was negatively charged (Table 2) suggesting stable colloidal dispersion due to inter particular repulsion. This is due to the presence of the carboxylic group on the polymer backbone and PEGMA ester bond delocalization.[42] In the case of DOX loaded nanoparticles decrease of zeta potential indicates the entrapment of positively

© 2021 The Author(s). Published by the Royal Society of Chemistry

Open Access Article. Published on 07 kvtna 2021. Downloaded on 15.04.2026 15:36:47.
This article is licensed under a Creative Commons Attribution-NonCommercial 3.0 Unported Licence.

Table 2 Hydrodynamic Size and zeta potential of the core–shell nanoparticle with or without DOX

	Size (nm)	PDI	Zeta potential
BCP10	148.9 ± 8	0.363 ± 0.03	−24.1 ± 7
BCP25	167.8 ± 3	0.323 ± 0.07	−42.4 ± 3
BCP50	181.4 ± 7	0.318 ± 0.02	−36.8 ± 3
BCP10-DOX	199.3 ± 3	0.231 ± 0.04	−19 ± 3
BCP25-DOX	210.3 ± 11	0.511 ± 0.01	−13.7 ± 1
BCP50-DOX	255 ± 6	0.666 ± 0.01	−12.9 ± 4

Table 3 % DOX loading (DL%) and % entrapment efficiency (EE%) of different polymer

	Mass ratio (polymer : DOX)	DOX feed (mg)	DL%	EE%
BCP10	1 : 0.1	10	2.53	10.75
BCP25	1 : 0.5	10	5.1	30.6
BCP50	1 : 1	10	5.98	38.87

charged DOX which diminishes the negative charge acquired by the nanoparticles.

Drug loading and release study

Physical entrapment of hydrophobic DOX to a hydrophobic core of the core–shell nanoparticle is dependent upon the hydrophobe chain length and the quantity. Here we have synthesized polymers with an increased segment of stearic acid in BCP10, BCP25, and BCP50. All the polymers have been investigated with drug loading (%) and drug encapsulation efficiency (%) with different polymer/DOX mass ratio.

It is found that DOX entrapment is proportional with the increase of stearic acid content that is BCP10 shows only 2.53% drug loading and BCP25, BCP50 shows higher drug loading capability with 5.1% and 5.98% drug loading while the mass ratio is 1 : 1 (polymer : DOX) (data shown in Table 3). Similarly, maximum drug loading efficiency attained up to 38.87% for BCP50, and the obtained result can stem from the presence of long-chain lipid molecular structure to the backbone of the hybrid polymer. Indeed, hybrid polymers having long chain hydrophobic structures can accommodate more hydrophobic drugs to their core due to strong hydrophobic interaction.[33,39] Further, the DOX loading was confirmed by UV-Vis spectroscopy and DOX shows its characteristic absorption peak at $\lambda = 481$ nm (0.5 mg ml^{-1}) (Fig. 4a), furthermore the characteristic red fluorescence due to DOX was also observed inside the cell under CLSM images (Fig. 4b) which confirms the successful entrapment of DOX into the nanoparticles. However, comparing to polymer–drug conjugates, BCPs show higher drug loading capability.[14,43,44]

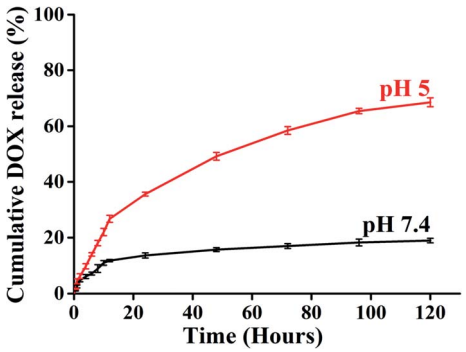

Fig. 5 DOX release from BCP50-DOX at pH 7.4 and pH 5.

A key feature of a nanoparticle for cancer therapeutics should be sustained release with minimal DOX release to the normal tissue site to escape the cytotoxic effect associated with anticancer drugs. Time-dependent drug release at different pH environments were also assessed to evaluate the drug release behaviour of BCP50 as it has shown maximum drug loading. The DOX release experiment was performed at pH 7.4 and 5 at 37 °C to simulate the condition during transport through systemic circulation and to mimic the cytosolic environment of a tumor cell respectively. The cumulative release profile (%) of DOX was observed for 120 hours (5 days) and the 68% maximum drug release was observed for BCP50 at acidic pH 5 and 18% drug release at blood pH *i.e.* 7.4 (Fig. 5).

Initial burst release was observed during first 12 hours which suggests the concentration-dependent diffusion of DOX

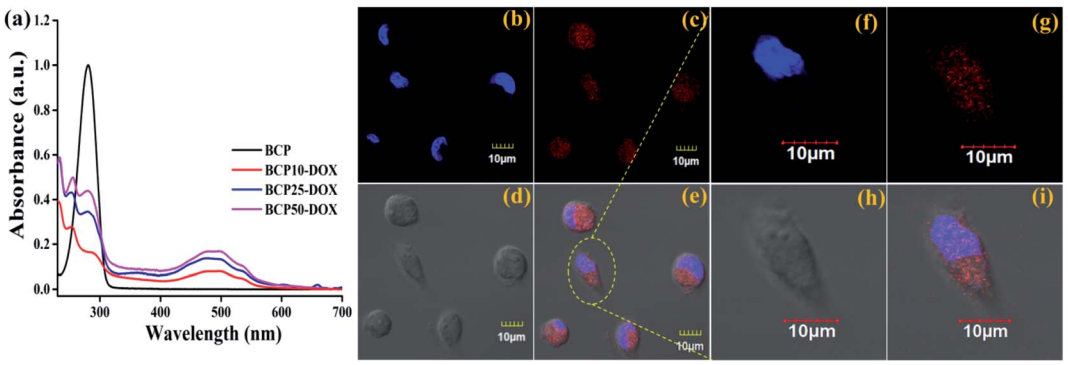

Fig. 4 (a) UV-Vis spectrum of blank polymer and DOX loaded polymer; position of DOX loaded nanoparticle inside the cell. Where (b) nucleus stained by DAPI, (c) DOX loaded BCP50 (d) bright field image, (e) merged image and (f–i) shows the expanded view of a single cell.

Open Access Article. Published on 07 kvtna 2021. Downloaded on 15.04.2026 15:36:47.
This article is licensed under a Creative Commons Attribution-NonCommercial 3.0 Unported Licence.

released from the core. After that, the slow-release pattern attributes to the stearic acid hydrophobic core which enables the very slow entry of endosomal enzymes to the core and slow hydrolysis of ester bonds present in SEMA as the ester bond undergoes hydrolysis in acidic condition.[39] Different release kinetic models were also employed to understand the drug release mechanism from the nanoparticle matrix. To evaluate the DOX release mechanism we have studied the zero order, first order, Hixon–Crowell, Korsmeyer–Peppas, and Higuchi kinetic models to estimate the regression coefficient values (R^2) which are shown in Table 4 with the corresponding graph Fig. S4(a–e) and S5(a–e).† It was observed Korsmeyer–Peppas kinetics model shows maximum R^2 value for both acidic and neutral pH and the values for pH 7.4 and 5 is 0.895 and 0.969 respectively. Meanwhile, the release exponent (n) was also found 0.454 and 0.642 which also suggest the non-Fickian diffusion or anomalous diffusion as the n value is lies between $0.43 < n < 0.85$ (ref. [45] and [46]) which is consistent with the previous report.[47]

Cytotoxicity study. MTT assay was performed using MDA-MB-231 cancer cells to evaluate the cytotoxicity of all the synthesized BCPs. The cells were incubated with different copolymer concentrations ranging from 10–500 μg ml^{-1}. Fig. 7a shows no significant toxicity with all the three polymers after 24 hours of the incubation period. As we have increased the fatty acid content to the copolymer, that may increase the biocompatibility as fatty acids are one of the key components of cells.

***In vitro* cellular uptake.** In this study, the cellular uptake of all the DOX loaded BCPs (BCP10, BCP25, BCP50) were investigated using confocal laser scanning microscopy (CLSM). We also have interpreted the 3D interactive plot to estimate the DOX intensity (a.u.) and correlate them to understand the DOX loading effect in different BCPs. The CLSM images (Fig. 6) depicts the DOX loaded polymers (BCP10-DOX, BCP25-DOX, BCP50-DOX) that were successfully uptaken by the cells within 4 hours at 37 °C. The blue fluorescence was observed due to the selective nucleus staining by DAPI (Fig. 6a–c) and substantial strong red fluorescence inside the cytoplasm as well as nuclei (Fig. 4b) was also observed due to the inherent DOX fluorescence. As a result Fig. 6a1, b1and c1 showed the respective CLSM images of BCP10-DOX, BCP25-DOX and BCP50-DOX where a strong red fluorescence inside the cytoplasm was observed. The 3D interactive plot (Fig. 6a4–c4) was generated and DOX fluorescence intensity was estimated by image j software (version-1.51k) (Fig. 6a5–c5) which indicated the increased DOX intensity with the increase of hydrophobic repeating unit of SEMA. It is in agreement with DOX loading study that BCPs containing more DOX, will show more fluorescence intensity. Among the nanoparticles BCP50-DOX (Fig. 6c5) shows strong red fluorescent intensity for DOX, which also stands with a close agreement with maximum drug loading to BCP50-DOX. The successful uptake of the nanoparticles after 4 hours and the strong red fluorescence indicated these nanoparticles are capable to accumulate inside the cells. The hydrophobic modification may also greatly influence the uptake as the cell membrane is composed of the protein–lipid–protein (PLP) layer. Therefore, the lipid modification of the nanocarriers may increase the recognition of the nanoparticle to the cell which led to the ease of uptake.

***In vitro* anticancer activity.** *In vitro* anticancer activity of DOX loaded BCPs was evaluated and compared against the activity of free DOX. The obtained results (Fig. 7b) suggest that maximum growth inhibition of cancer cells by free DOX was 16% where 35%, 28%, and 20% viable cells were observed by BCP10-DOX, BCP25-DOX, and BCP50-DOX respectively after 24 hours of incubation. Furthermore, the DOX release could be facilitated by hydrolysis of ester linkage between SA and HEMA by the endosomal acidic environment (pH 4.0–5.0) which led to concrete the anticancer effect by reaching the therapeutic window. Similar results were also obtained by Wei *et al.*[33] Fig. 7c shows the observed IC_{50} value for each formulation and free DOX. BCP50-DOX (1.748 ± 0.103 μg) and free DOX (3.759 ± 0.162 μg) shows a significant cytotoxic effect while compared to other DOX loaded nanoparticle (data shown in Table S1†). Furthermore, IC_{50} values obtained by BCP50-DOX also much lower than free DOX (1 μg of BCP50-DOX contain 0.0598 μg free DOX), where 0.1074 μg equivalent amount of DOX can show a similar result obtained by 3.759 μg of free DOX. The obtained results indicate that the BCP50-DOX is more effective compared to free DOX in terms of inhibiting cell proliferation. All the MTT result shows BCP50 with or without DOX is the desired nanoparticle for DOX delivery.

Cellular morphology study. To understand the cell death SEM analysis is become an important observation in recent reports[48,49] which could be visually observed *via* the morphological change in the apoptotic cellular structure. So, we have further conducted the SEM analysis of treated or untreated cells to support the MTT assay where only 16% and 20% viable cells

Table 4 Regression coefficient values (R^2) of BCP50-DOX at different kinetic model at pH 7.4 and 5

	pH 7.4		pH 5.6	
Kinetic models	R^2	Equation	R^2	Equation
Zero order	0.692	$y = 0.136x + 5.853$	0.884	$y = 0.578x + 10.487$
First order	0.718	$y = 0.0007x + 5.853$	0.956	$y = -0.0043x + 1.957$
Hixon–Crowell	0.353	$y = 0.011x + 1.601$	0.565	$y = 0.0230x + 1.949$
Korsmeyer–Peppas	0.895	$y = 0.454x + 0.453$	0.969	$y = 0.642x + 0.610$
Higuchi	0.890	$y = 1.712x + 2.677$	0.907	$y = 6.819x - 1.156$

© 2021 The Author(s). Published by the Royal Society of Chemistry

Open Access Article. Published on 07 kvtna 2021. Downloaded on 15.04.2026 15:36:47.
This article is licensed under a Creative Commons Attribution-NonCommercial 3.0 Unported Licence.

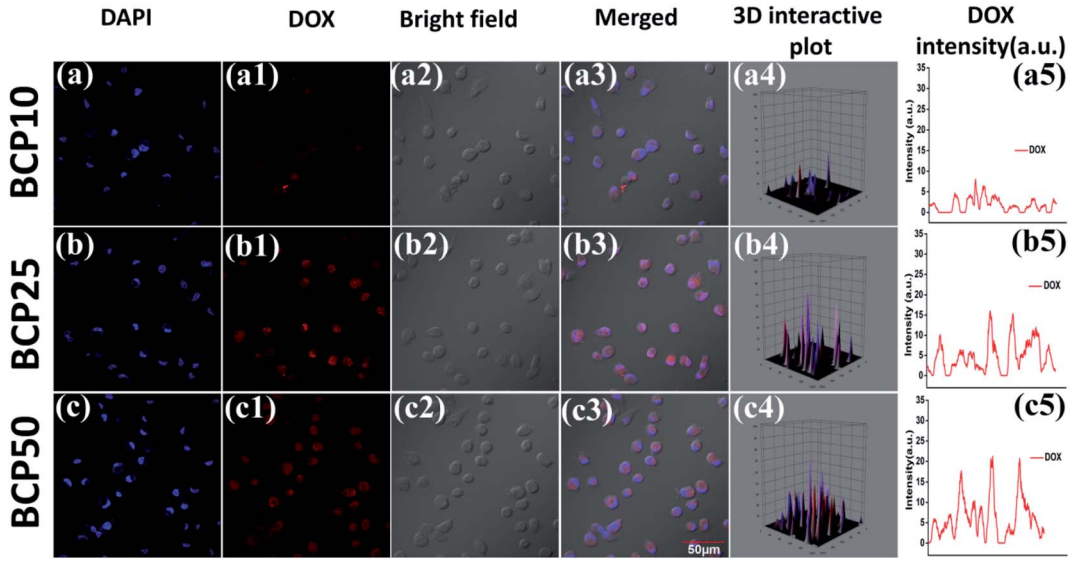

Fig. 6 Confocal microscopy images of fixed MDA MB-231 cells incubated with BCP10-DOX, BCP25-DOX and BCP50-DOX for 4 hours. Where (a)–(c) corresponds to the stained nucleus by DAPI. Similarly, (a1)–(c1) are the corresponding confocal images of cells which shows successful uptake of DOX loaded nanoparticle. (a2)–(c2) are the bright field images of the corresponding cells. (a3)–(c3) are the merged images where purple colour shows co-localization of the blue and red colour due to DAPI and DOX fluorescence which suggests successful uptake of the DOX loaded nanoparticle. (a4)–(c4) are the 3D interactive plots of intracellular DOX and DAPI fluorescence and (a5)–(c5) are the measured intracellular DOX intensity.

were observed for free DOX and BCP50-DOX respectively. We have observed the surface topographies of cells under SEM (ZEISS EVO-MA 10) after 24 hours of exposure to the free DOX and BCP50-DOX at 37 °C in a CO_2 incubator. The cellular structure with or without treatment were shown in Fig. 8. In this study, Fig. 8a–c are the cellular structure referred to as control or untreated, free DOX treated and BCP50-DOX treated cells. It is a general concern that the apoptosis of a cell involves cell shrinkage and blebbing.[50] In Fig. 8a the cell without treatment shows regular anatomical morphology with distinct dendron like lamellipodia,[51] whereas free DOX treated cell (Fig. 8b) shows the cellular necrosis, and the fragment of apoptotic

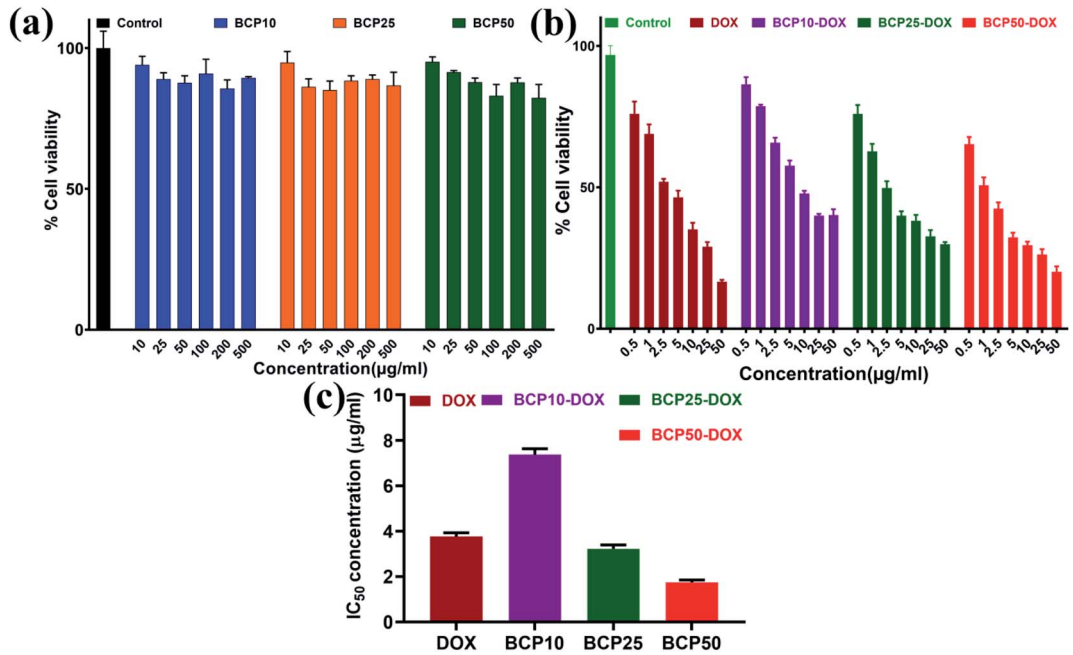

Fig. 7 (a) Cell viability assay of BCP10, BCP25 and BCP50 using MDA-MB-231 cell line; (b) MTT assay of free DOX and DOX loaded P(PEGMA-*co*-SEMA) block co-polymer (BCP10-DOX, BCP25-DOX, BCP50-DOX); (c) determined 50% inhibitory concentration (IC_{50}) value of DOX, BCP10-DOX, BCP25-DOX, BCP50-DOX.

© 2021 The Author(s). Published by the Royal Society of Chemistry

Open Access Article. Published on 07 kvtna 2021. Downloaded on 15.04.2026 15:36:47.
This article is licensed under a Creative Commons Attribution-NonCommercial 3.0 Unported Licence.

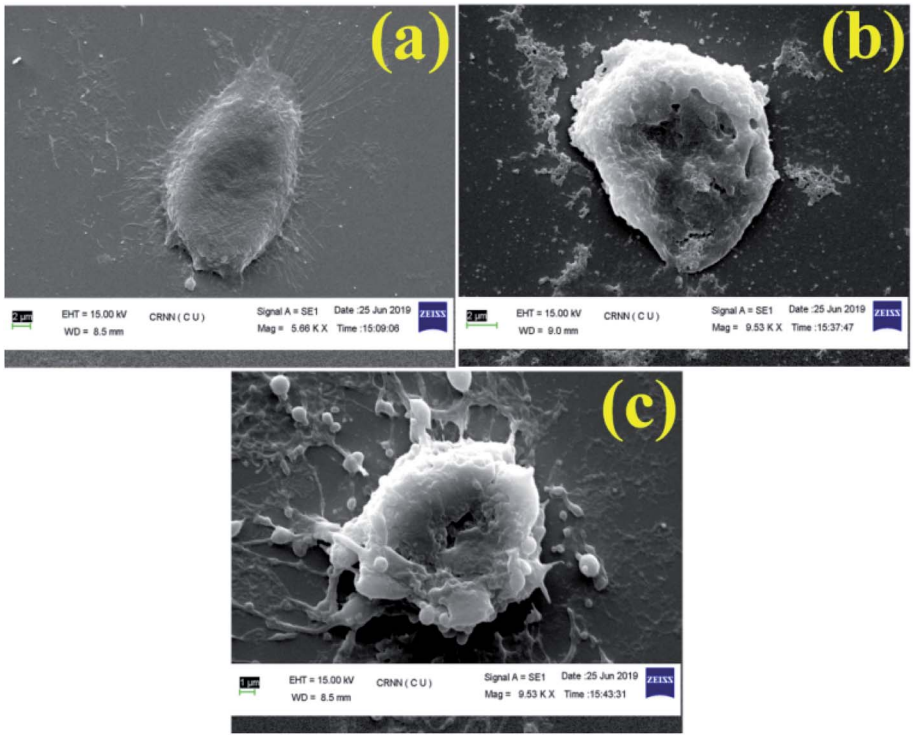

Fig. 8 Cellular morphology under SEM, where (a) control (without treatment) (b) DOX treated and (c) BCP50-DOX treated cells.

bodies is scattered around as free DOX is highly cytotoxic. In the case of BCP50-DOX (Fig. 8c), the cell shrinkage with blebbing and the ruptured cell membrane is observed with inhibition of lamellipodia formation due to the anticancer effect of BCP50-DOX. Similar results were also obtained by Basu *et al.*[36] DOX treated cells also show apoptosis which may happen in the case of non-cancerous cells as the free DOX is a very small-sized (1.5 nm) molecular entity structure and could be uptaken through the tight endothelial junction. However, wrapping the DOX by a nanostructure may restrict the accumulation within the normal cell with minimal damage as the drug release in the non-acidic media is very low.[52,53] Thus the DOX loaded nanoparticle shows its anticancer activity by damaging the organelle along with the membrane integrity of the cancer cell.

Conclusion

In this study, we have designed a core shell nano template by using PEGMA and SEMA *via* RAFT polymerization for DOX delivery to MDA MB-231 cancer cell. PEGMA served as the corona or outer shell and SEMA formed the inner hydrophobic core which helps to entrap substantial amount of DOX by strong hydrophobic interaction. The increase in hydrophobic segment showed increase in hydrodynamic diameter of the particle without significant cytotoxic effect upto a relatively higher concentration (0.5 mg ml^{-1}). Furthermore, SEMA content greatly influences the drug loading and release from the inner core. *In vitro* cellular uptake also indicated successful internalization of the DOX loaded BCPs with increased DOX fluorescence intensity with the increase of SEMA. The *in vitro* anticancer activity also suggested that the nanoparticle can effectively deliver DOX to the cancer cells. Apoptic cell death was also observed from SEM study. Most of the anticancer drugs are hydrophobic in nature and possess very low bioavailability due to solubility issues. Thus, wrapping them by an amphiphilic polymer containing lipid segment may improve their bio-distribution along with better access to the cancer environment. These results indicated that BCP50 could be a promising nanomaterial for hydrophobic anticancer drug delivery system in near future.

Conflicts of interest

The authors have no conflict of interest.

Acknowledgements

KS acknowledges to DST-SERB through two sanctioned projects EEQ/2016/000712 and ECR/2016/002018 and also acknowledges UGC for UGC-BSR Research Start-Up Grant (F.30-363/2017(BSR), Dt-08/08/2017) and. PS acknowledges UGC for RGNF-SC fellowship (RGNF-2014-15-SC-TRI-67257). RS acknowledges CU for UPE-II Nanofabrication project fund (UGC/166/UPE-II, Dt-03/04/2017) for financial support. PS also acknowledge Debajit Maiti, Department of Chemistry, Shiv Nadar University, Uttar Pradesh, India for providing NMR facility.

References

1 W. Smulders and M. J. Monteiro, *Macromolecules*, 2004, **37**, 4474–4483.

© 2021 The Author(s). Published by the Royal Society of Chemistry

Open Access Article. Published on 07 kvtna 2021. Downloaded on 15.04.2026 15:36:47.
This article is licensed under a Creative Commons Attribution-NonCommercial 3.0 Unported Licence.

2 S. L. Banerjee, M. Khamrai, K. Sarkar, N. K. Singha and P. Kundu, *Int. J. Biol. Macromol.*, 2016, **85**, 157–167.
3 D. Sutton, N. Nasongkla, E. Blanco and J. Gao, *Pharm. Res.*, 2007, **24**, 1029–1046.
4 M. Licciardi, G. Cavallaro, M. Di Stefano, C. Fiorica and G. Giammona, *Macromol. Biosci.*, 2011, **11**, 445–454.
5 N. Corrigan, K. Jung, G. Moad, C. J. Hawker, K. Matyjaszewski and C. Boyer, *Prog. Polym. Sci.*, 2020, 101311.
6 J. Jennings, G. He, S. M. Howdle and P. B. Zetterlund, *Chem. Soc. Rev.*, 2016, **45**, 5055–5084.
7 K. Miyata, R. J. Christie and K. Kataoka, *React. Funct. Polym.*, 2011, **71**, 227–234.
8 B. Mandal, H. Bhattacharjee, N. Mittal, H. Sah, P. Balabathula, L. A. Thoma and G. C. Wood, *Nanomed. Nanotechnol. Biol. Med.*, 2013, **9**, 474–491.
9 H. L. Wong, R. Bendayan, A. M. Rauth and X. Y. Wu, *J. Controlled Release*, 2006, **116**, 275–284.
10 Y. Li, H. L. Wong, A. J. Shuhendler, A. M. Rauth and X. Y. Wu, *J. Controlled Release*, 2008, **128**, 60–70.
11 K. Ghosal, S. Ghosh, D. Ghosh and K. Sarkar, *Int. J. Biol. Macromol.*, 2020, **162**, 1605–1615.
12 P. Jana, S. Ghosh and K. Sarkar, *Int. J. Biol. Macromol.*, 2020, **161**, 1149–1160.
13 S. Ghosh, K. Ghosal, S. A. Mohammad and K. Sarkar, *Chem. Eng. J.*, 2019, **373**, 468–484.
14 D. Yu, P. Peng, S. S. Dharap, Y. Wang, M. Mehlig, P. Chandna, H. Zhao, D. Filpula, K. Yang and V. Borowski, *J. Controlled Release*, 2005, **110**, 90–102.
15 K. Ghosal and K. Sarkar, *ACS Biomater. Sci. Eng.*, 2018, **4**, 2653–2703.
16 K. Ghosal and A. Ghosh, *Mater. Sci. Eng. C*, 2019, **96**, 887–903.
17 Q. Gao, Q. Liang, F. Yu, J. Xu, Q. Zhao and B. Sun, *Colloids Surf., B*, 2011, **88**, 741–748.
18 K. Sarkar, S. L. Banerjee, P. Kundu, G. Madras and K. Chatterjee, *J. Mater. Chem. B*, 2015, **3**, 5266–5276.
19 Y. Y. Yang, Y. Wang, R. Powell and P. Chan, *Clin. Exp. Pharmacol. Physiol.*, 2006, **33**, 557–562.
20 G. Prencipe, S. M. Tabakman, K. Welsher, Z. Liu, A. P. Goodwin, L. Zhang, J. Henry and H. Dai, *J. Am. Chem. Soc.*, 2009, **131**, 4783–4787.
21 A. Szymborska and H. Gerhardt, *Cold Spring Harbor Perspect. Biol.*, 2018, **10**, a029223.
22 H. Yuan, L.-J. Lu, Y.-Z. Du and F.-Q. Hu, *Mol. Pharmaceutics*, 2011, **8**, 225–238.
23 F.-Q. Hu, X.-l. Wu, Y.-Z. Du, J. You and H. Yuan, *Eur. J. Pharm. Biopharm.*, 2008, **69**, 117–125.
24 K. Ulbrich, Č. Koňák, Z. Tuzar and J. Kopeček, *Macromol. Chem. Phys.*, 1987, **188**, 1261–1272.
25 Z. Ahmad, A. Shah, M. Siddiq and H.-B. Kraatz, *RSC Adv.*, 2014, **4**, 17028–17038.
26 S. S. Hallan, P. Kaur, V. Kaur, N. Mishra and B. Vaidya, *Artif. Cells Nanomed. Biotechnol.*, 2016, **44**, 334–349.
27 R. Greenwald, *J. Controlled Release*, 2001, **74**, 159–171.
28 G. Kwon, S. Suwa, M. Yokoyama, T. Okano, Y. Sakurai and K. Kataoka, *J. Controlled Release*, 1994, **29**, 17–23.
29 M. J. Joralemon, S. McRae and T. Emrick, *Chem. Commun.*, 2010, **46**, 1377–1393.
30 X. Sun, R. Rossin, J. L. Turner, M. L. Becker, M. J. Joralemon, M. J. Welch and K. L. Wooley, *Biomacromolecules*, 2005, **6**, 2541–2554.
31 R. Saha, S. Bhayye, S. Ghosh, A. Saha and K. Sarkar, *ACS Appl. Bio Mater.*, 2019, **2**, 5349–5365.
32 B. Maiti and P. De, *RSC Adv.*, 2013, **3**, 24983–24990.
33 T. Wei, C. Chen, J. Liu, C. Liu, P. Posocco, X. Liu, Q. Cheng, S. Huo, Z. Liang and M. Fermeglia, *Proc. Natl. Acad. Sci.*, 2015, **112**, 2978–2983.
34 A. O. Costa, C. N. Lunardi and A. J. Gomes, *Curr. Nanomed.*, 2020, **10**, 63–75.
35 S. Ghosh, S. Das, A. K. De, N. Kar and T. Bera, *RSC Adv.*, 2017, **7**, 29575–29590.
36 A. Basu, P. Upadhyay, A. Ghosh, D. Chattopadhyay and A. Adhikary, *ACS Biomater. Sci. Eng.*, 2018, **5**, 373–389.
37 K. G. Goswami, B. Saha, S. Mete and P. De, *Macromol. Chem. Phys.*, 2018, **219**, 1800398.
38 B. Maiti, S. Maiti and P. De, *RSC Adv.*, 2016, **6**, 19322–19330.
39 P. Laskar, B. Saha, S. K. Ghosh and J. Dey, *RSC Adv.*, 2015, **5**, 16265–16276.
40 S. S. Jena, S. G. Roy, V. Azmeera and P. De, *React. Funct. Polym.*, 2016, **99**, 26–34.
41 C. Maiti, S. Parida, S. Kayal, S. Maiti, M. Mandal and D. Dhara, *ACS Appl. Mater. Interfaces*, 2018, **10**, 5318–5330.
42 F. Quaglia, L. Ostacolo, G. De Rosa, M. I. La Rotonda, M. Ammendola, G. Nese, G. Maglio, R. Palumbo and C. Vauthier, *Int. J. Pharm.*, 2006, **324**, 56–66.
43 R. B. Greenwald, Y. H. Choe, J. McGuire and C. D. Conover, *Adv. Drug Delivery Rev.*, 2003, **55**, 217–250.
44 E. Jäger, A. Jäger, P. Chytil, T. Etrych, B. Říhová, F. C. Giacomelli, P. Štěpánek and K. Ulbrich, *J. Controlled Release*, 2013, **165**, 153–161.
45 J. Siepmann and N. Peppas, *Adv. Drug Delivery Rev.*, 2001, **48**, 165.
46 S. Ghosh, N. Kar and T. Bera, *Int. J. Biol. Macromol.*, 2016, **93**, 961–970.
47 X. Jin, Q. Wang, J. Sun, H. Panezai, S. Bai and X. Wu, *Microporous Mesoporous Mater.*, 2017, **254**, 77–85.
48 S. De, K. Patra, D. Ghosh, K. Dutta, A. Dey, G. Sarkar, J. Maiti, A. Basu, D. Rana and D. Chattopadhyay, *ACS Biomater. Sci. Eng.*, 2018, **4**, 514–531.
49 S. Ghorai, I. Roy, S. De, P. S. Dash, A. Basu and D. Chattopadhyay, *New J. Chem.*, 2020, **44**, 5366–5376.
50 N. Pipan and M. Sterle, *Cell Tissue Res.*, 1986, **246**, 647–652.
51 A. Zafar, S. Singh, Y. K. Satija, D. Saluja and I. Naseem, *Toxicol. In Vitro*, 2018, **46**, 19–28.
52 K. M. Ibiyeye, A. B. Z. Zuki, N. Nordin and M. Ajat, *Front. Radiat. Oncol.*, 2019, **9**, 599.
53 P. Sarkar, S. Ghosh and K. Sarkar, *Colloids Surf., B*, 2020, **197**, 111382.

© 2021 The Author(s). Published by the Royal Society of Chemistry